nanomaterials

MDPI

Article

Nitrogen-Containing Gas Sensing Properties of 2-D Ti_2N and Its Derivative Nanosheets: Electronic Structures Insight

Hongni Zhang [1,2], Wenzheng Du [1], Jianjun Zhang [1], Rajeev Ahuja [3,4] and Zhao Qian [1,*]

[1] Key Laboratory of Liquid-Solid Structural Evolution and Processing of Materials (Ministry of Education), Shandong University, Jinan 250061, China; nini810@126.com (H.Z.); 201813740@mail.sdu.edu.cn (W.D.); 15163625981@163.com (J.Z.)
[2] College of Industry and Commerce, Shandong Management University, Jinan 250357, China
[3] Condensed Matter Theory, Department of Physics and Astronomy, Ångström Laboratory, Uppsala University, 75120 Uppsala, Sweden; rajeev.ahuja@physics.uu.se
[4] Department of Materials Science and Engineering, KTH Royal Institute of Technology, 10044 Stockholm, Sweden
* Correspondence: qianzhao@sdu.edu.cn

Abstract: In this work, the potentials of two-dimensional Ti_2N and its derivative nanosheets Ti_2NT_2(T=O, F, OH) for some harmful nitrogen-containing gas (NCG) adsorption and sensing applications have been unveiled based on the quantum-mechanical Density Functional Theory calculations. It is found that the interactions between pure Ti_2N and NCGs (including NO, NO_2, and NH_3 in this study) are very strong, in which NO and NO_2 can even be dissociated, and this would poison the substrate of Ti_2N monolayer and affect the stability of the sensing material. For the monolayer of Ti_2NT_2(T=O, F, OH) that is terminated by functional groups on surface, the adsorption energies of NCGs are greatly reduced, and a large amount of charges are transferred to the functional group, which is beneficial to the reversibility of the sensing material. The significant changes in work function imply the good sensitivity of the above mentioned materials. In addition, the fast response time further consolidates the prospect of two-dimensional Ti_2NT_2 as efficient NCGs' sensing materials. This theoretical study would supply physical insight into the NCGs' sensing mechanism of Ti_2N based nanosheets and help experimentalists to design better 2-D materials for gas adsorption or sensing applications.

Keywords: atomic structure; electronic structure; Density Functional Theory (DFT); MXenes; two-dimensional materials

Citation: Zhang, H.; Du, W.; Zhang, J.; Ahuja, R.; Qian, Z. Nitrogen-Containing Gas Sensing Properties of 2-D Ti_2N and Its Derivative Nanosheets: Electronic Structures Insight. *Nanomaterials* **2021**, *11*, 2459. https://doi.org/10.3390/nano11092459

Academic Editor: Jihoon Lee

Received: 12 August 2021
Accepted: 14 September 2021
Published: 21 September 2021

1. Introduction

Industrial pollutant emissions account for a large share of environmental pollution, and one of the most harmful is nitrogen-containing gas (NCGs), such as NO, NO_2, and NH_3. At the same time, the nitrogen-containing gases themselves are generally toxic and can damage the respiratory cells of humans and animals [1–4]. Therefore, there is an urgent need to explore efficient and alternative materials for the sensing or capturing of these gases. Although some current solid-state sensors can also detect toxic gases, there is still much room for improvement due to the increasingly high demand for sensitivity, selectivity, stability, and other factors [5,6]. Two-dimensional (2-D) materials have large contact areas with gas and special electronic properties; thus, their interactions with gas molecules have been widely studied, especially in gas sensing and capturing [7]. For example, Zhang et al. studied the adsorption behavior between four modified graphene substrates and small gas molecules (CO, NO, NO_2, and NH_3) and significantly improved the performance of the gas sensor by introducing doping or defects [8]. Liu et al. found that the GeSe monolayer had potential for NH_3 gas capture and storage, as well as for the detection and catalysis of SO_2 and NO_2. The optical properties of this GeSe monolayer can also be tuned as a candidate

material for optical sensors by adsorbing different small molecules [9]. Li et al. compared the structures and electronic properties of pure and two vacancy-defected MoS_2 nanosheets with NO adsorption. Defects can effectively improve the NO-sensing performance [10].

Transition metal carbide or nitride MXenes are also one family of promising gas-sensing materials [11,12], where M is a transition metal and X is carbon or nitrogen. The general formula of MXenes is written as M_nX_{n-1}. During the preparation process in an aqueous solution containing fluoride ions, there may be some O, F, and OH functional groups formed [13–15]. This type of MXene with functional groups is written as $M_nX_{n-1}T_n$(T=O, F, OH). MXenes are also widely reported in energy storage, electrode materials, ion batteries, and the spintronic and optical devices, due to their unique structures and properties [16–24].

After our review of previous literature, we found that some carbide-based MXenes have the potential to be used as sensors for molecules, such as amino acids and nucleobase [25,26]. With less exfoliation energy compared with other types, the synthesizability of the nitride MXenes is good [27], while there are fewer studies on their use in sensing NCGs [28–32]. In order to obtain a theoretical understanding of the nitride MXenes in terms of their sensing or capturing performance towards nitrogen-containing gas (NCGs), in this work, we conducted a detailed computational study on the adsorption behaviors of NCGs (including NO, NO_2, and NH_3) of Ti_2N monolayer with bare surface and terminated with O, F, and OH functional groups. Density Functional Theory–based first-principles calculations were performed to unveil the adsorption structures, charge transfer, band structures, density of states, and work functions to stimulate and inspire the deep mechanism investigations.

2. Methods

DFT calculations were employed by using the projector augmented wave (PAW) [33] pseudo-potentials in a Vienna *Ab initio* Simulation Package (VASP) [34]. For the exchange-correlation functional, we used the Perdew-Burke-Ernzerhof (PBE) [35] form of the generalized gradient approximation (GGA). Grimme's DFT-D2 method was used to describe the van der Waals interactions [36]. This method adds semi-empirical dispersion on the basis of conventional Kohn–Sham DFT energy. In calculations, Ti_2N and Ti_2NT_2(T=O, F, OH) were constructed as $4 \times 4 \times 1$ supercells, and a 20 Å vacuum layer was added in *Z*-axis direction to eliminate the interlayer interaction. The energy cutoff of 520 eV was used for wave functions' expansion. The Brillouin zone integration was sampled with 5×5 **k**-grid mesh for geometry optimizations and 15×15 **k**-grid mesh for electronic properties calculations to achieve high accuracy. Geometry optimizations were performed by using the conjugated gradient method, and the convergence criterion was set to be 0.02 eV/Å on force and 1×10^{-5} eV/atom on energy. The adsorption energy (E_{ads}) of nitrogen-containing gas (NCGs) on Ti_2N or Ti_2NT_2(T=O, F, OH) is defined as follows:

$$E_{ads} = E_{MXene + NCGs} - E_{NCGs} - E_{MXene} \quad (1)$$

where E_{ads}, $E_{MXene + NCGs}$, E_{MXene}, and E_{NCGs} stand for the adsorption energy, total energies of optimized Ti_2N or Ti_2NT_2(T=O, F, OH) MXene with adsorbed NCGs molecules, energies of pure MXene, and isolated NCGs (NO, NO_2, and NH_3) molecules respectively.

3. Results and Discussion

First of all, the Ti_2N MXene has a hexagonal structure with three layers of atoms: the middle is N-atoms layer; and the upper (a) and lower (b) layers are Ti atoms, as is shown in Figure 1a. After structural optimizations, the Ti-N bond length is 2.07 Å, the bond angle of the same layer Ti and N (Ti–N–Ti) and N–Ti–N are both 92.4°, and the bond angle of different-layer Ti and N (Ti–N–Ti) is 87.6°. The lattice parameter of the 4×4 supercell is a = b = 11.98 Å. These parameters are very consistent with the results of Ti_2N studied in other works in the literature [37,38], indicating the reliability of the calculation results. The band structure and PDOS of the material are shown in Figure 1b; it can be seen that there

are many electronic states available for occupation at the Fermi level, and Ti_2N exhibits metallic properties. The states near the Fermi level are occupied by Ti electrons, where N's contribution is relatively small, meaning that low-energy carriers mainly originate from Ti.

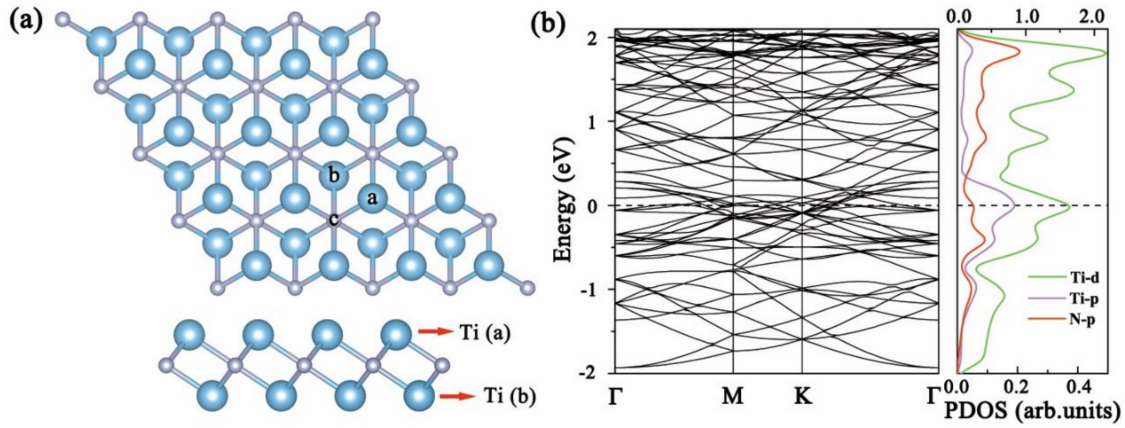

Figure 1. (**a**) Top and side view of the optimized structures for Ti_2N monolayer (blue and silver balls represent Ti and N atoms, respectively). (**b**) Band structure and projected density of states of Ti_2N monolayer (Ti*d*-orbital uses top abscissa and other orbitals use bottom coordinate).

In order to study the most stable adsorption configurations of NCGs on Ti_2N MXene, the NO, NO_2, and NH_3 molecules were respectively placed at three different adsorption sites, namely on top of the Ti(a) atom shown in Figure 1a (site "a"), on top of the hollow Ti(b) atom (site "b"), or on top of the N atom (site "c"). The screened most stable configurations after adsorbing NCGs are shown in Figure 2. Both NO and NO_2 show dissociative adsorption. The adsorption energy is far greater than those of other two-dimensional materials [39–44]. When NO is adsorbed on Ti_2N, N and O atoms are adsorbed at the adjacent site "b" respectively. The distance between N and O is 3.07 Å, which is much larger than 1.15 Å of free NO gas molecule, indicating that the N–O bond is broken and NO dissociates. The dissociated N and O atoms form new bonds with Ti atoms in the upper layer of Ti_2N, with bond lengths of 1.93 and 1.97 Å, respectively. Ti atoms protrude slightly upwards from its binding, and the Ti–N bond length on the surrounding matrix increases by about 0.14 Å. It can be seen from Figure 3a that, after dissociation, the N 2*p* and O 2*p* in NO and the nearby Ti 3*d*-orbitals have similar peak positions and obvious *p*-*d* hybridization in PDOS diagram. There is a strong bonding between NO and Ti_2N, and the adsorption energy is as high as −9.809 eV. At the same time, the band structure shows that the dissociative adsorption of NO on Ti_2N does not change the original metallic properties.

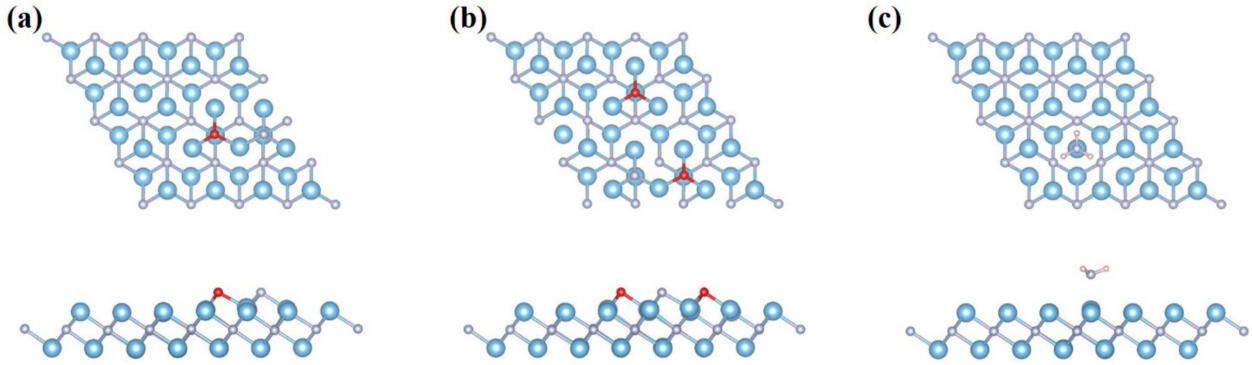

Figure 2. Top and side view of the optimized atomic structures for Ti_2N monolayer after adsorbing (**a**) NO, (**b**) NO_2, and (**c**) NH_3 (blue, silver, red, and pink balls represent Ti, N, O, and H atoms, respectively).

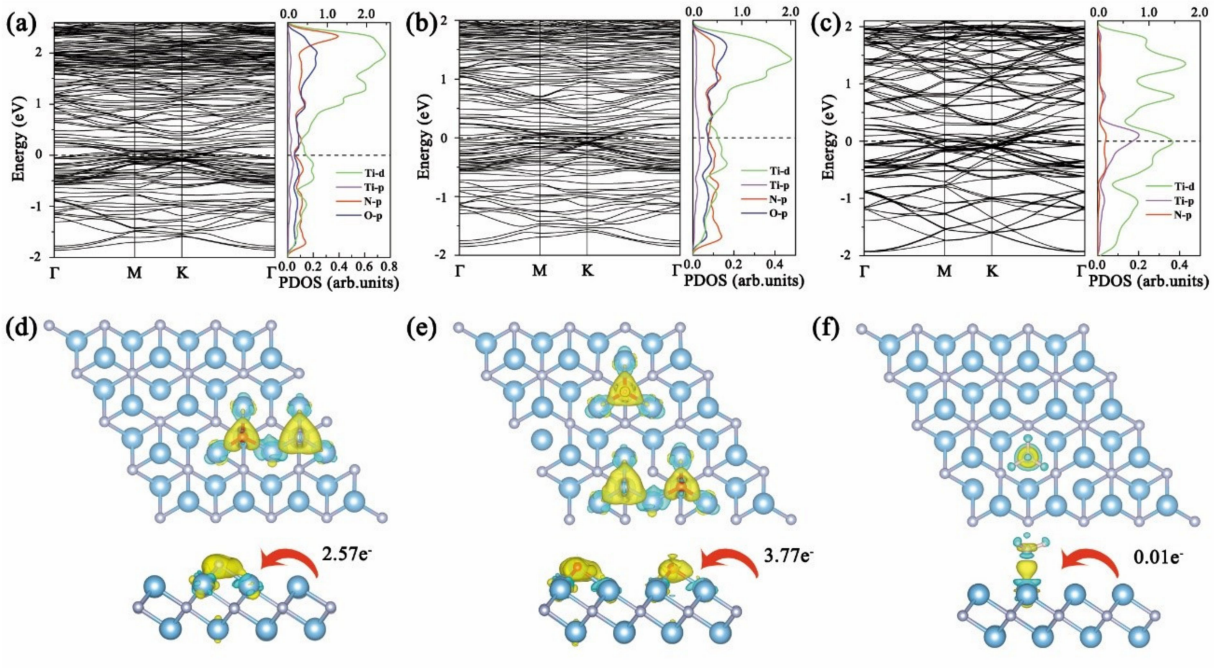

Figure 3. Band structures, PDOS and differential charge densities of Ti_2N after adsorbing (**a**,**d**) NO, (**b**,**e**) NO_2, and (**c**,**f**) NH_3 (Ti*d*-orbital uses top abscissa and other orbitals use bottom coordinate; isovalue of NO and NO_2 is set to 0.01 e/Å^3, NH_3 is set to 0.005 e/Å^3).

When NO_2 interacts with Ti_2N, it is interesting that NO_2will also dissociate similar to NO adsorption, and all the N and O atoms are adsorbed at the site "b". One O-atom keeps the same shape adsorbed at adjacent position, while the another O-atom is adsorbed away from it. The N-O bond length in $NO_2$is increased to 3.07 Å. The dissociative adsorption energy is up to −14.336 eV. As can be seen from the electronic structure in Figure 3b, the *p*-*d* hybridization of N 2*p*-, O 2*p*-, and Ti 3*d*-orbitals corresponds with the strong bonding of Ti-N and Ti-O, respectively. The metallic behavior of Ti_2N remains after NO_2 dissociative adsorption. From the differential charge density in Figure 3d–f, it can be seen that the dissociation of NO and NO_2 is caused by the excessive charge transfer from Ti_2N MXene to the gas molecule. The Bader charge analysis shows that 2.57 e^- and 3.77 e^- charges were transferred from Ti_2N to NO and NO_2, respectively. The bulk of these transferred charges comes from the surrounding Ti atoms, and this is also the fundamental reason why the N-O bond is broken.

The adsorption of NH_3 is completely different from those of NO and NO_2. It is bound by associative adsorption with the binding distance of 2.2 Å and the E_{ads} value of−1.286 eV. As shown in Figure 3c, NH_3 tends to be adsorbed at site "a" with N-atom below and three H-atoms evenly distributed above. The distance between the Ti atom at site "a" and the surrounding N atom is elongated to 2.14 Å, and the N–Ti–N bond angle is reduced to 88.3°. To figure out the binding and charge transfer mechanism between NH_3 molecule and Ti_2N monolayer, the band structure and PDOS were analyzed. It is difficult to find a pronounced overlap between N *p* and Ti*d* close to the Fermi level in Figure 3c. The amount of charge transfer is only 0.01 e^-, which is far less than those of NO and NO_2. The bonding between NH_3 and Ti_2N is very weak, and the band structure that is almost the same as the bare Ti_2N monolayer also confirms this.

For ideal gas sensing application, excessive adsorption energy is obviously not feasible. The dissociative adsorption of NO and NO_2 on Ti_2N monolayer will obviously poison the substrate and make it fail to work cyclically. The dissociation of gas molecules results from the strong interaction between the bare Ti_2N surface and O atoms. Thus, the pure Ti_2N monolayer can be used as a kind of gas-trapping material instead of highly efficient sensor for NO and NO_2. Compared with those two gases, the adsorption effect of NH_3

is satisfactory. The associative adsorption with lower energy will not cause chemical poisoning, which is beneficial to Ti_2N as a promising candidate material for reversible NH_3 sensors. In actual preparation process, some functional groups are usually introduced onto the Ti_2N monolayer, and these functional groups may have significant impacts on adsorption properties of the material. Considering this reality, in the following part, we recount how we studied the adsorption behaviors of the Ti_2N monolayer terminated by O, F, and OH towards NCGs.

We introduce O, F, and OH functional groups at three adsorption positions (site "a", "b", and "c") of Ti_2N, of which OH only considers the vertical direction (O atom is close to the matrix). All the functional groups tend to adsorb at site "b" with the lowest energy, as shown in Figure 4a–c. After adsorbing different functional groups, the Ti–N bonds show different degrees of extension: 2.164, 2.052, and 2.065 Å for Ti_2NO_2,Ti_2NF_2, and $Ti_2N(OH)_2$, respectively, which is due to the bonding between Ti and functional groups. Gouveia et al. reported possible atomic-layer-stacking-phase transitions of some MXenes [41]; thus, we also carefully checked this point in our research. It is found that the material system maintains phase stability and stacking way after introduction of those functional groups. The Bader charge analysis shows that 1.1, 0.8, and 0.8 e^- are respectively transferred to O, F, and OH from Ti_2N. It can also be observed in Figure 4d–f that there is a strong overlap between the Ti*d*-orbital and the T (O, F, or OH)*d*-orbitals.

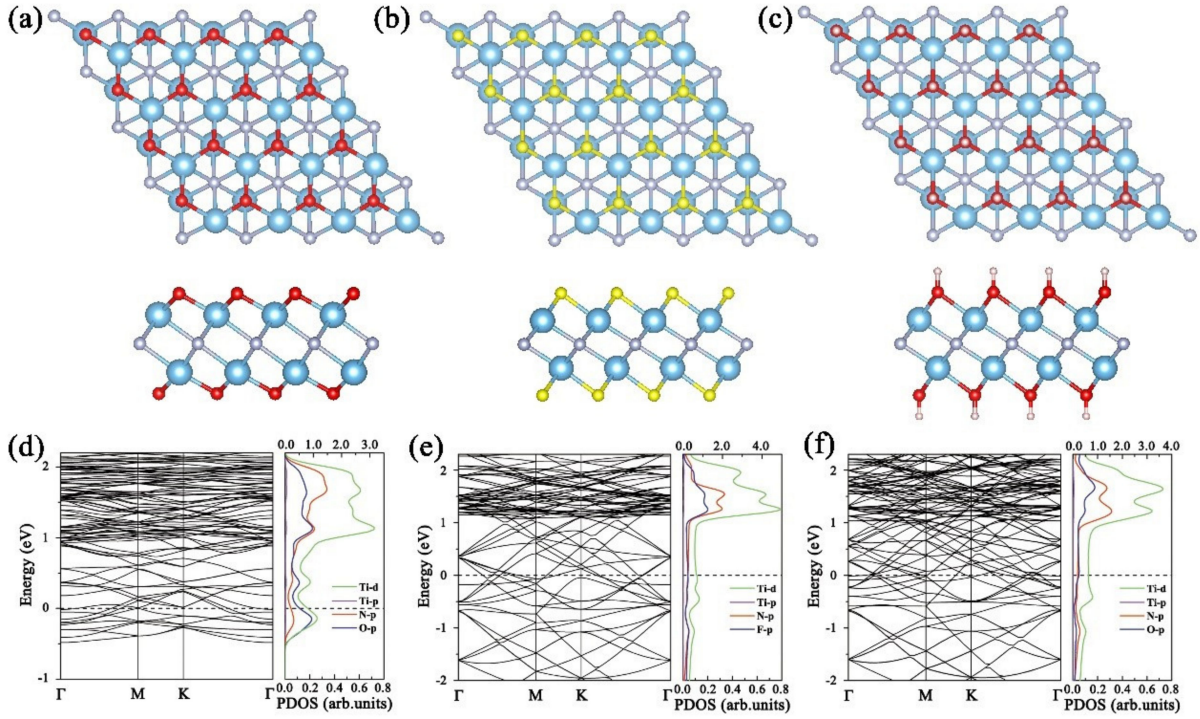

Figure 4. Top and side view of the optimized structures, band structures, and PDOS of (**a**,**d**) Ti_2NO_2, (**b**,**e**) Ti_2NF_2, and (**c**,**f**) $Ti_2N(OH)_2$ monolayers (blue, silver, red, pink, and yellow balls represent Ti, N, O, H, and F atoms, respectively. Ti*d*-orbital uses top abscissa and other orbitals use bottom coordinate).

After obtaining the stable configurations of Ti_2NT_2(T=O, F, OH), we placed various NCGs molecules at different adsorption sites (site "a", "b", and "c"), such as those in pure Ti_2N. It can be seen from the most stable adsorption structures after optimizations in Figure 5 that all NCGs have no dissociative adsorption on Ti_2NT_2(T=O, F, OH). The binding distance is defined as the shortest direct distance between the NCGs molecule and the matrix; hereby, the binding distances of NO, NO_2, and NH_3 on Ti_2NO_2 are 2.082, 1.824, and 2.172 Å, respectively. The bond lengths of NO and NH_3 after adsorption are the same as those of free gas molecules, while one of the N–O bonds of NO_2 is stretched to 1.530 Å.

The 2-D Ti_2NO_2 does not change significantly under NO environment, while the Ti atoms exposed to the adsorption positions of NO_2 and NH_3 are obviously dragged out. For NCGs adsorption on the surface of Ti_2NF_2, the molecular bond lengths and the matrix are almost unchanged with the adsorption distances of 2.951, 2.800, and 2.947 Å, respectively. It is surprising when NO is adsorbed on $Ti_2N(OH)_2$. The H atoms on the substrate bind with NO, where three H atoms combine with the N atom and one H atom combines with the O atom to form a hydroxyl lammonium-like product. The adsorption distances of NO_2 and $NH_3$are 1.625 and 1.702 Å, which are measured from the nearest H atom; thus, they are shorter than those of other Ti_2NT_2(T=O, F). While, the adsorption is not strong, especially the NH_3 molecule has basically no change compared with the free molecule.

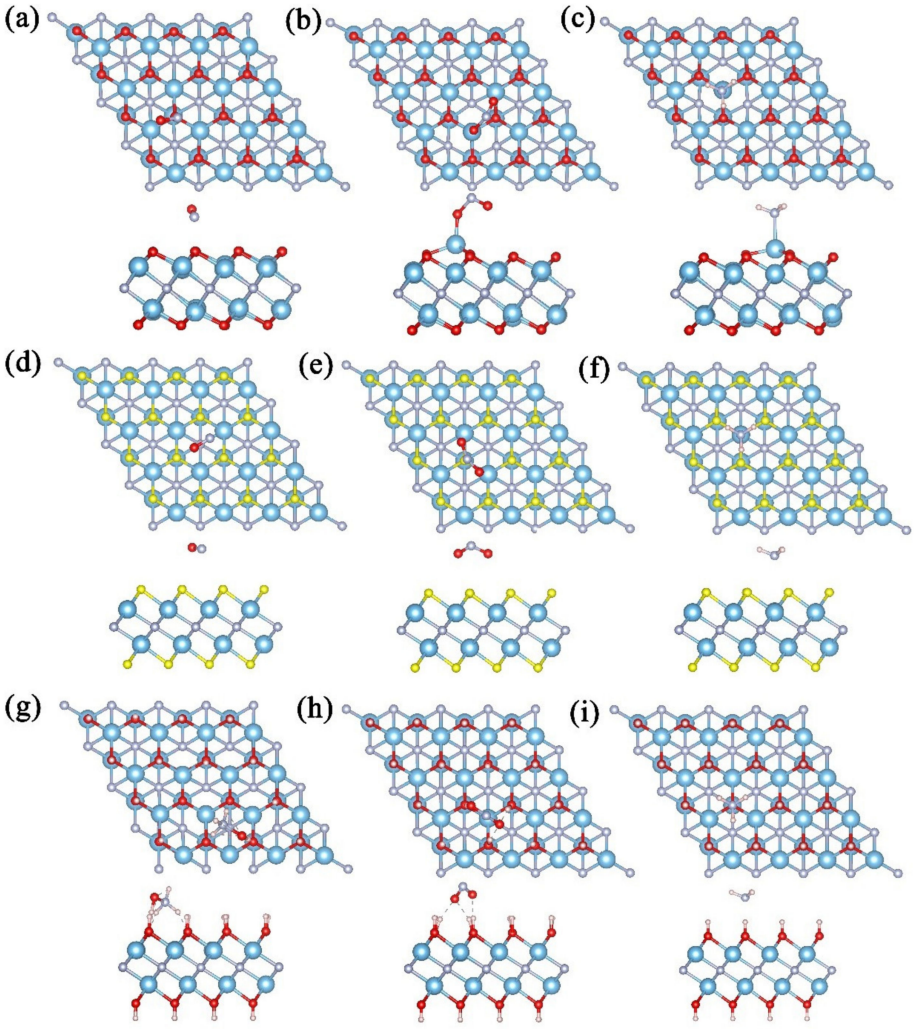

Figure 5. Top and side view of the optimized structures for Ti_2NO_2 after adsorbing (**a**) NO, (**b**) NO_2, and (**c**) NH_3; Ti_2NF_2 after adsorbing (**d**) NO, (**e**) NO_2, and (**f**) NH_3;and $Ti_2N(OH)_2$ after adsorbing (**g**) NO, (**h**) NO_2, and (**i**) NH_3 (blue, silver, red, pink, and yellow balls represent Ti, N, O, H, and F atoms, respectively).

We can clearly see that the absolute values of adsorption energy of NCGs on Ti_2NT_2(T=O, F, OH) decrease sharply compared with the pure substrate in Table 1, especially on the surface of Ti_2NF_2. Since the H atoms of the OH functional groups fall off the $Ti_2N(OH)_2$ substrate and bind with NO, their decrease is not that large. On the pure Ti_2N monolayer, a large amount of charge is transferred from Ti_2N to NO and NO_2. After the introduction of the functional group O, F, or OH, most of the charge transfer from Ti_2N is captured by these functional groups, which leaves a very small charge amount for exchange with NCGs.

In addition, one can see that the difference in adsorption energy of each NCG on substrate is obvious, indicating that the selectivity is good. As mentioned above, NO and NO_2 are dissociatively adsorbed on pure Ti_2N, which results in the poisoning of the Ti_2N surface. Similarly, NO binds with H atoms of $Ti_2N(OH)_2$ and destroys the surface integrity of the substrate, which is detrimental to the sensing material. Thus, $Ti_2N(OH)_2$ is not suitable for NO sensing. From the perspective of adsorption energy, those of NO on Ti_2NO_2, NO_2on Ti_2NF_2, and NH_3on $Ti_2N(OH)_2$ are between physisorption and chemisorption, which are important to make sensors work reversibly and increase their efficiency [45].

Table 1. Adsorption energy (E_{ads}) and charge-transfer profiles of NCGs adsorption on 2-D Ti_2N and Ti_2NT_2(T=O, F, OH).

NCGs	Adsorption Energy (eV)				Charge Transfer (e^-)			
	Ti_2N	Ti_2NO_2	Ti_2NF_2	$Ti_2N(OH)_2$	Ti_2N	Ti_2NO_2	Ti_2NF_2	$Ti_2N(OH)_2$
NO	−9.81	−0.68	−0.15	−5.55	2.57	−0.24	−0.07	0.50
NO_2	−14.34	−2.38	−0.36	−3.78	3.77	0.49	0.29	1.78
NH_3	−1.29	−1.16	−0.13	−0.57	0.01	−0.18	−0.03	0.15

To better understand the effects of NCGs molecules on Ti_2NT_2(T=O, F, OH), the band structure and PDOS of all the adsorption systems are calculated and shown in Figure 6. Regardless of the type of NCGs adsorption, the system retains metallic properties. Only when Ti_2NO_2 is exposed to NO_2, the Ti*d*-, O*p*-,and N *p*-orbitals show a certain degree of d-p hybridization, while the *p*- and *d*-orbitals in other PDOS do not overlap. When Ti_2NO_2 adsorbs NO, a flat band appears near the Fermi energy and indicates that the electrons are delocalized, which further proves that the interaction between NO and Ti_2NO_2 is not strong. This phenomenon is more obvious when NCGs are adsorbed on Ti_2NF_2 shown in Figure 6d–f. These results are consistent with the above discussion on energetics and charge-transfer profiles.

An ideal sensing material not only needs to possess excellent gas-binding capability but also has a requirement for good sensitivity. The conductivity of materials, especially two-dimensional materials, is closely related with work function. During adsorption, if the electron affinity of gas molecule surpasses the work function of substrate materials, the molecule will grab electrons from the surface of materials and the molecule would be charged negatively; in contrast, the adsorbed molecule would be charged positively. Both two cases would change the electronic structure, as well as conductivity of materials. The work function [46] is defined as the least energy required to free an electron from the surface of a system, which can be calculated by the following equation:

$$\varphi = V_\infty - E_f \quad (2)$$

where φ, V_∞, and E_f are the work function, electrostatic potential at the vacuum level, and the Fermi energy, respectively. Figure 7 shows the change of work function of Ti_2N and Ti_2NT_2(T=O, F, OH) before and after adsorption of various NCGs. "Bare" represents the bare system (before adsorption), and the names of NCGs in abscissa represent various systems after adsorption of different gases. The work functions of Ti_2NO_2 and $Ti_2N(OH)_2$ decrease obviously after adsorbing NO, while that of Ti_2NF_2 increases significantly after adsorbing NO_2. After adsorbing NH_3, the work functions of Ti_2N, Ti_2NF_2, and Ti_2NO_2 all decrease, and the change of Ti_2NO_2 is the most obvious. Because all the systems are metallic, even small changes in work function can cause large variation in conductivity [43]. Comprehensively considering the above results on adsorption structure and energy, Ti_2NO_2 can be used as a superior sensing candidate material for NO and NH_3, and Ti_2NF_2 can be utilized as that for NO_2. In addition, the potential of sensing properties of Ti_2N, Ti_2NF_2, and $Ti_2N(OH)_2$ towards NH_3 is also good.

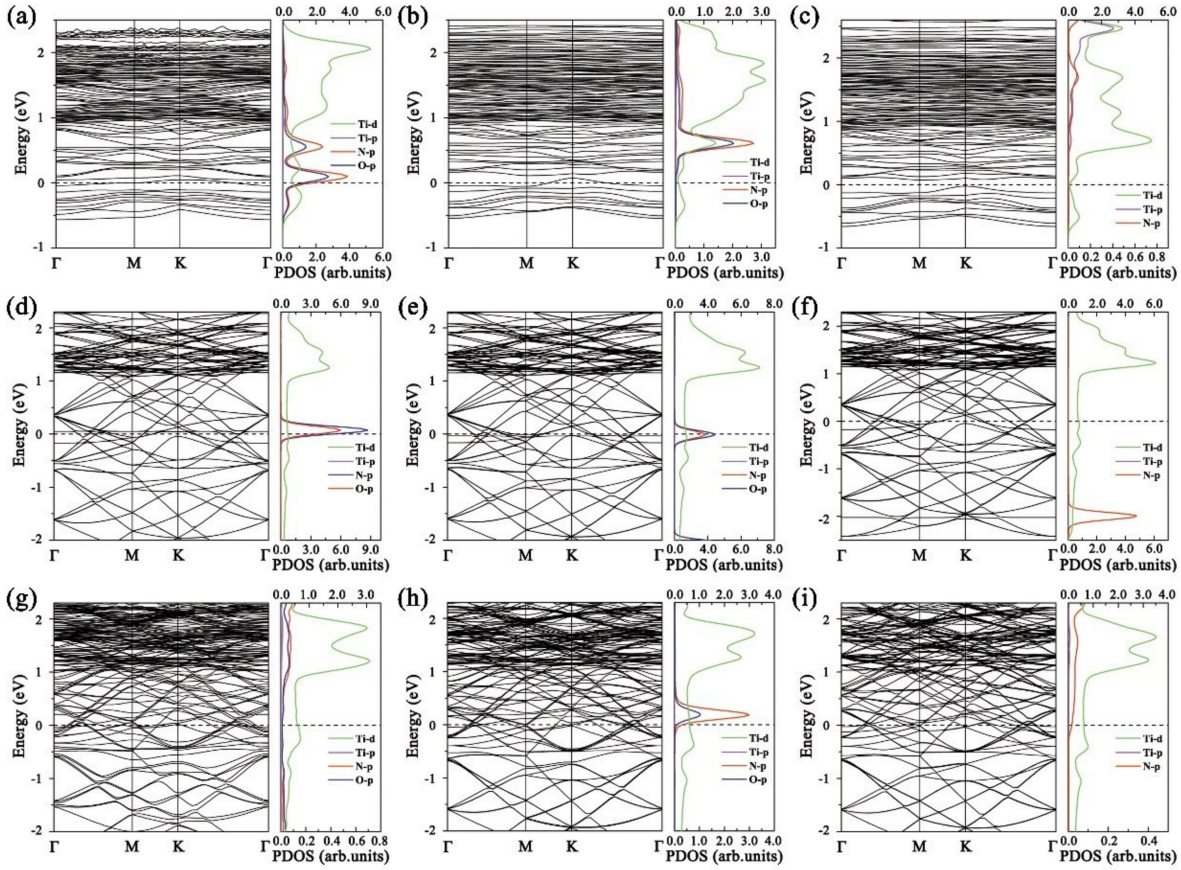

Figure 6. Band structures and PDOS of Ti_2NO_2 after adsorbing (**a**) NO, (**b**) NO_2, and (**c**) NH_3; Ti_2NF_2 after adsorbing (**d**) NO, (**e**) NO_2, and (**f**) NH_3; $Ti_2N(OH)_2$ after adsorbing (**g**) NO, (**h**) NO_2, and (**i**) NH_3 (Ti*d*-orbital uses top abscissa and other orbitals use bottom coordinate).

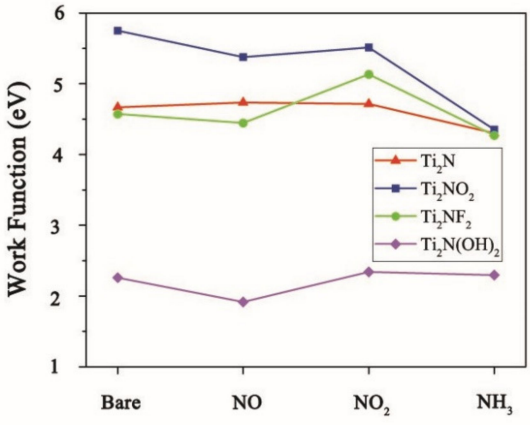

Figure 7. Work function change of Ti_2N and Ti_2NT_2(T=O, F, OH) before and after adsorption of various NCGs.

Finally, we discuss the recovery time (τ). An ideal gas-sensing material needs appropriate adsorption energy, and a shorter recovery time is better. To make a gas sensor work efficiently, a short recovery time is required. It can be calculated through transition state theory, namely by the following relationship [47,48]:

$$\tau = \upsilon^{-1}\exp(-E_{ads}/kT) \quad (3)$$

where υ, E_{ads}, k, and T are the attempt frequency, adsorption energy, Boltzmann's constant (8.62×10^{-5} eV K^{-1}), and operational temperature, respectively. Under the same conditions, the increase in adsorption energy will lead to an exponential increase in recovery time; then the higher operating temperature compensation is required, which is detrimental to the sensor performance. In order to get a relatively reasonable value, we set the attempt frequency here to $10^{12}s^{-1}$ based on traditional transition state theory [49–51]. The recovery time of NO on Ti_2NO_2 is calculated to be 2.16 $\times$ 10^5 us, and that of NO_2/Ti_2NF_2 and NH_3/Ti_2NF_2 is 1.29 and 1.71 $\times 10^{-4}$ us, respectively. Here it can be seen in Figure 8 that the adsorption energy difference of less than 1 eV can be enlarged to several orders of magnitude in recovery time. Although NO on Ti_2NO_2 has the longest recovery time, the value is only 0.216 s. For the system of NH_3/Ti_2NF_2, it has the shortest recovery time, which shows that the MXene system in this research can be promising. Therefore, when other conditions are met, the candidate materials with appropriate gas adsorption energy and short response time should be selected.

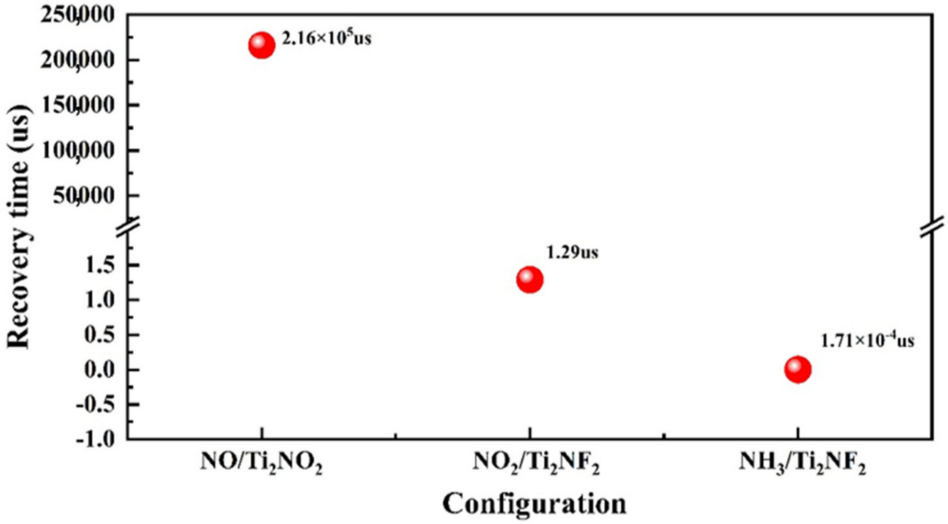

Figure 8. Recovery time of different sensing systems.

4. Summary and Outlook

In this work, we used the first-principles DFT calculations to investigate the 2-D Ti_2N nanosheet and its Ti_2NT_2(T=O, F, OH) derivative materials for harmful nitrogen-containing gas (NGCs) adsorption and sensing applications. When NCGs are exposed on the surface of Ti_2N, the dissociative adsorption of NO and NO_2 occurs and destroys the stability of the nanosheet, which would make it hard to work reversibly, while NH_3 does not have this effect on Ti_2N. When studying the interaction mechanisms between NCGs and Ti_2NT_2(T=O, F, OH), it can be found that a large amount of charges accumulates at functional groups, thus greatly reducing the adsorption energy of NCGs in absolute value. The obvious change in work function, coupled with the metallic nature of the systems, would improve gas sensitivity. Appropriate gas adsorption energy can directly determine fast recovery time to ensure the efficiency and reversibility of sensors. This research gives the electronic structures origin and application prospect of Ti_2NT_2(T=O, F, OH) as efficient NCGs sensing materials and would inspire experimentalists to explore better 2-D candidates in the field.

Author Contributions: Formal analysis, H.Z., W.D., J.Z., R.A., and Z.Q.; project administration, Z.Q.; supervision, Z.Q.; writing—original draft, H.Z., W.D., and Z.Q.; writing—review and editing, H.Z. and Z.Q.; funding acquisition, Z.Q. All authors have read and agreed to the published version of the manuscript.

Funding: We are grateful for the support from the Natural Science Foundation of China (51801113 and 52171182), the Sino-German Center for Research Promotion and NSFC (GZ1673), the Natural

Science Foundation of Shandong Province (ZR2018MEM001), the Young Scholars Program of Shandong University (YSPSDU), the Education Program of Shandong University (2020Y299), and the Fundamental Research Funds for the Central Universities.

Data Availability Statement: Data are contained within the article.

Acknowledgments: The National Supercomputer Centre (NSC) and the HPC Cloud Platform of Shandong University are acknowledged.

Conflicts of Interest: The authors declare no conflict of interest.

References

1. Ramanathan, V.; Feng, Y. Air pollution, greenhouse gases and climate change: Global and regional perspectives. *Atmos. Environ.* **2009**, *43*, 37–50. [CrossRef]
2. Koolen, C.D.; Rothenberg, G. Air pollution in Europe. *ChemSusChem* **2018**, *12*, 164–172. [CrossRef]
3. Hasselblad, V.; Eddy, D.M.; Kotchmar, D.J. Synthesis of environmental evidence: Nitrogen dioxide epidemiology studies. *J. Air Waste Manag. Assoc.* **1992**, *42*, 662–671. [CrossRef]
4. Garrett, M.H.; Hooper, M.A.; Hooper, B.M.; Abramson, M.J. Respiratory symptoms in children and indoor exposure to nitrogen dioxide and gas stoves. *Am. J. Respir. Crit. Care Med.* **1998**, *158*, 891–895. [CrossRef] [PubMed]
5. Ouyang, T.; Qian, Z.; Ahuja, R.; Liu, X. First-principles investigation of CO adsorption on pristine, C-doped and N-vacancy defected hexagonal AlN nanosheets. *Appl. Surf. Sci.* **2018**, *439*, 196–201. [CrossRef]
6. Liu, Y.; Parisi, J.; Sun, X.; Lei, Y. Solid-state gas sensors for high temperature applications—A review. *J. Mater. Chem. A* **2014**, *2*, 9919–9943. [CrossRef]
7. Tang, X.; Du, A.; Kou, L. Gas sensing and capturing based on two-dimensional layered materials: Overview from theoretical perspective. *Wiley Interdiscip. Rev. Comput. Mol. Sci.* **2018**, *8*, e1361. [CrossRef]
8. Zhang, Y.-H.; Chen, Y.-B.; Zhou, K.-G.; Liu, C.; Zeng, J.; Zhang, H.-L.; Peng, Y. Improving gas sensing properties of graphene by introducing dopants and defects: A first-principles study. *Nanotechnology* **2009**, *20*, 185504. [CrossRef]
9. Liu, L.; Yang, Q.; Wang, Z.; Ye, H.; Chen, X.; Fan, X.; Zhang, G. High Selective Gas Detection for small molecules based on Germanium selenide monolayer. *Appl. Surf. Sci.* **2018**, *433*, 575–581. [CrossRef]
10. Li, F.; Shi, C. NO-sensing performance of vacancy defective monolayer MoS_2 predicted by density function theory. *Appl. Surf. Sci.* **2018**, *434*, 294–306. [CrossRef]
11. Yu, X.-F.; Li, Y.-C.; Cheng, J.-B.; Liu, Z.-B.; Li, Q.-Z.; Li, W.-Z.; Yang, X.; Xiao, B. Monolayer Ti_2CO_2: A Promising Candidate for NH_3 Sensor or Capturer with High Sensitivity and Selectivity. *ACS Appl. Mater. Interfaces* **2015**, *7*, 13707–13713. [CrossRef]
12. Xiao, B.; Li, Y.-C.; Yu, X.-F.; Cheng, J.-B. MXenes: Reusable materials for NH_3 sensor or capturer by controlling the charge injection. *Sens. Actuators B Chem.* **2016**, *235*, 103–109. [CrossRef]
13. Naguib, M.; Kurtoglu, M.; Presser, V.; Lu, J.; Niu, J.; Heon, M.; Hultman, L.; Gogotsi, Y.; Barsoum, M.W. Two-dimensional nanocrystals produced by exfoliation of Ti_3AlC_2. *Adv. Mater.* **2011**, *23*, 4248–4253. [CrossRef] [PubMed]
14. Naguib, M.; Mashtalir, O.; Carle, J.; Presser, V.; Lu, J.; Hultman, L.; Gogotsi, Y.; Barsoum, M.W. Two-dimensional transition metal carbides. *ACS Nano* **2012**, *6*, 1322–1331. [CrossRef]
15. Feng, A.; Yu, Y.; Wang, Y.; Jiang, F.; Yu, Y.; Mi, L.; Song, L. Two-dimensional MXene Ti_3C_2 produced by exfoliation of Ti_3AlC_2. *Mater. Des.* **2017**, *114*, 161–166. [CrossRef]
16. Lashgari, H.; Abolhassani, M.; Boochani, A.; Elahi, S.; Khodadadi, J. Electronic and optical properties of 2D graphene-like compounds titanium carbides and nitrides: DFT calculations. *Solid State Commun.* **2014**, *195*, 61–69. [CrossRef]
17. Weng, H.; Ranjbar, A.; Liang, Y.; Song, Z.; Khazaei, M.; Yunoki, S.; Arai, M.; Kawazoe, Y.; Fang, Z.; Dai, X. Large-gap two-dimensional topological insulator in oxygen functionalized MXene. *Phys. Rev. B* **2015**, *92*, 075436–0754367. [CrossRef]
18. Pan, H. Electronic properties and lithium storage capacities of two-dimensional transition-metal nitride monolayers. *J. Mater. Chem. A* **2015**, *3*, 21486–21493. [CrossRef]
19. Wang, D.; Liu, Y.; Meng, X.; Wei, Y.; Zhao, Y.; Pang, Q.; Chen, G. Two-dimensional VS_2 monolayers as potential anode materials for lithium-ion batteries and beyond: First-principles calculations. *J. Mater. Chem. A* **2017**, *5*, 21370–21377. [CrossRef]
20. Kumar, H.; Frey, N.C.; Dong, L.; Anasori, B.; Gogotsi, Y.; Shenoy, V.B. Tunable magnetism and transport properties in nitride MXenes. *ACS Nano* **2017**, *11*, 7648–7655. [CrossRef]
21. Yang, Z.; Zheng, Y.; Li, W.; Zhang, J. Investigation of two-dimensional hf-based MXenes as the anode materials for li/na-ion batteries: A DFT study. *J. Comput. Chem.* **2019**, *40*, 1352–1359. [CrossRef] [PubMed]
22. Gao, G.; Ding, G.; Li, J.; Yao, K.; Wu, M.; Guangqian, D. Monolayer MXenes: Promising half-metals and spin gapless semiconductors. *Nanoscale* **2016**, *8*, 8986–8994. [CrossRef] [PubMed]
23. Pang, J.; Mendes, R.G.; Bachmatiuk, A.; Zhao, L.; Ta, H.Q.; Gemming, T.; Liu, H.; Liu, Z.; Rummeli, M.H. Applications of 2D MXenes in energy conversion and storage systems. *Chem. Soc. Rev.* **2018**, *48*, 72–133. [CrossRef] [PubMed]
24. Shukla, V.; Jena, N.K.; Naqvi, S.R.; Luo, W.; Ahuja, R. Modelling high-performing batteries with Mxenes: The case of S-functionalized two-dimensional nitride Mxene electrode. *Nano Energy* **2019**, *58*, 877–885. [CrossRef]

25. Gouveia, J.; Novell-Leruth, G.; Vines, F.; Illas, F.; Gomes, J. The Ti_2CO_2MXene as a nucleobase 2D sensor: A first-principles study. *Appl. Surf. Sci.* **2021**, *544*, 148946. [CrossRef]
26. Gouveia, J.; Novell-Leruth, G.; Reis, P.M.L.S.; Viñes, F.; Illas, F.; Gomes, J. First-principles calculations on the adsorption behavior of amino acids on a titanium carbide MXene. *ACS Appl. Biol. Mater.* **2020**, *3*, 5913–5921. [CrossRef]
27. Dolz, D.; Morales-García, A.; Viñes, F.; Illas, F. Exfoliation energy as a descriptor of MXenes synthesizability and surface chemical activity. *Nanomaterials* **2021**, *11*, 127. [CrossRef] [PubMed]
28. Soundiraraju, B.; George, B.K. Two-dimensional Titanium Nitride (Ti2N) MXene: Synthesis, characterization, and potential application as surface-enhanced ramanscattering substrate. *ACS Nano* **2017**, *11*, 8892–8900. [CrossRef]
29. Li, Y.; Guo, Y.; Chen, W.; Jiao, Z.; Ma, S. Reversible hydrogen storage behaviors of Ti_2NMXenes predicted by first-principles calculations. *J. Mater. Sci.* **2018**, *54*, 493–505. [CrossRef]
30. Lin, H.; Yang, D.-D.; Lou, N.; Zhu, S.-G.; Li, H.-Z. Functionalized titanium nitride-based MXenes as promising host materials for lithium-sulfur batteries: A first principles study. *Ceram. Int.* **2018**, *45*, 1588–1594. [CrossRef]
31. Urbankowski, P.; Anasori, B.; Makaryan, T.; Er, D.; Kota, S.; Walsh, P.L.; Zhao, M.; Shenoy, V.B.; Barsoum, M.W.; Gogotsi, Y. Synthesis of two-dimensional titanium nitride Ti_4N_3(MXene). *Nanoscale* **2016**, *8*, 11385–11391. [CrossRef]
32. Xiao, X.; Yu, H.; Jin, H.; Wu, M.; Fang, Y.; Sun, J.; Hu, Z.; Li, T.; Wu, J.; Huang, L.; et al. Salt-templated synthesis of 2D metallic MoN and other nitrides. *ACS Nano* **2017**, *11*, 2180–2186. [CrossRef]
33. Blöchl, P.E. Projector augmented-wave method. *Phys. Rev. B* **1994**, *50*, 17953–17979. [CrossRef]
34. Kresse, G.; Joubert, D. From ultrasoft pseudopotentials to the projector augmented-wave method. *Phys. Rev. B* **1999**, *59*, 1758–1775. [CrossRef]
35. Perdew, J.P.; Burke, K.; Ernzerhof, M. Generalized gradient approximation made simple. *Phys. Rev. Lett.* **1996**, *77*, 3865–3868. [CrossRef]
36. Grimme, S. Semiempirical GGA-type density functional constructed with a long-range dispersion correction. *J. Comput. Chem.* **2006**, *27*, 1787–1799. [CrossRef]
37. Wang, D.; Gao, Y.; Liu, Y.; Jin, D.; Gogotsi, Y.; Meng, X.; Du, F.; Chen, G.; Wei, Y. First-principles calculations of Ti_2N and Ti_2NT_2 (T=O, F, OH) monolayers as potential anode materials for lithium-ion batteries and beyond. *J. Phys. Chem. C* **2017**, *121*, 13025–13034. [CrossRef]
38. Xie, Y.; Kent, P.R.C. Hybrid density functional study of structural and electronic properties of functionalized $Ti_{n+1}X_n$ (X=C, N) monolayers. *Phys. Rev. B* **2013**, *87*, 235441. [CrossRef]
39. Prasongkit, J.; Amorim, R.; Chakraborty, S.; Ahuja, R.; Scheicher, R.; Amornkitbamrung, V. Highly sensitive and selective gas detection based on silicene. *J. Phys. Chem. C* **2015**, *119*, 16934–16940. [CrossRef]
40. Leenaerts, O.; Partoens, B.; Peeters, F.M. Adsorption of H_2O, NH_3, CO, NO_2, and NO on graphene: A first-principles study. *Phys. Rev. B* **2008**, *77*, 125416. [CrossRef]
41. Gouveia, J.D.; Viñes, F.; Illas, F.; Gomes, J.R.B. MXenes atomic layer stacking phase transitions and their chemical activity consequences. *Phys. Rev. Mater.* **2020**, *4*, 054003. [CrossRef]
42. Ouyang, T.; Qian, Z.; Hao, X.; Ahuja, R.; Liu, X. Effect of defects on adsorption characteristics of AlN monolayer towards SO_2 and NO_2: Ab initio exposure. *Appl. Surf. Sci.* **2018**, *462*, 615–622. [CrossRef]
43. Kou, L.; Frauenheim, T.; Chen, C. Phosphorene as a superior gas sensor: Selective adsorption and distinct *I–V* response. *J. Phys. Chem. Lett.* **2014**, *5*, 2675–2681. [CrossRef] [PubMed]
44. Yue, Q.; Shao, Z.; Chang, S.; Li, J. Adsorption of gas molecules on monolayer MoS_2 and effect of applied electric field. *Nanoscale Res. Lett.* **2013**, *8*, 425. [CrossRef] [PubMed]
45. Hussain, T.; Singh, D.; Gupta, S.K.; Karton, A.; Sonvane, Y.; Ahuja, R. Efficient and selective sensing of nitrogen-containing gases by Si_2BN nanosheets under pristine and pre-oxidized conditions. *Appl. Surf. Sci.* **2018**, *469*, 775–780. [CrossRef]
46. Gholizadeh, R.; Yu, Y.-X. Work functions of pristine and heteroatom-doped graphenes under different external electric fields: An ab initio DFT study. *J. Phys. Chem. C* **2014**, *118*, 28274–28282. [CrossRef]
47. Barsan, N.; Koziej, D.; Weimar, U. Metal oxide-based gas sensor research: How to? *Sens. Actuators B Chem.* **2007**, *121*, 18–35. [CrossRef]
48. Nagarajan, V.; Chandiramouli, R. Investigation of NH_3 adsorption behavior on graphdiyne nanosheet and nanotubes: A first-principles study. *J. Mol. Liq.* **2018**, *249*, 24–32. [CrossRef]
49. Eyring, H. The activated complex in chemical reactions. *J. Chem. Phys.* **1935**, *3*, 107–115. [CrossRef]
50. Hadipour, N.L.; Peyghan, A.A.; Soleymanabadi, H. Theoretical study on the Al-doped ZnO nanoclusters for CO chemical sensors. *J. Phys. Chem. C* **2015**, *119*, 6398–6404. [CrossRef]
51. Ahmadi, A.; Hadipour, N.L.; Kamfiroozi, M.; Bagheri, Z. Theoretical study of aluminum nitride nanotubes for chemical sensing of formaldehyde. *Sens. Actuators B Chem.* **2012**, *161*, 1025–1029. [CrossRef]